npj | biomedical innovations

Article

https://doi.org/10.1038/s44385-025-00032-y

# Cracking the code: predicting tumor microenvironment enabled chemoresistance with machine learning in the human tumoroid models

Check for updates

Michael E. Bregenzer[1], Pooja Mehta[2], Kathleen M. Burkhard[1] & Geeta Mehta[1,2,3,4,5]

High-grade serous tubo-ovarian cancer (HGSC) is marked by substantial inter- and intra-tumor heterogeneity. The tumor microenvironments (TME) of HGSC show pronounced variability in cellular make-up across metastatic sites, which is linked to poorer patient outcomes. The influence of cellular composition on therapy sensitivity, including chemotherapy and targeted treatments, has not been thoroughly investigated. In this study, we examined the premise that the variations in cellular composition can forecast drug efficacy. Using a high-throughput 3D in vitro tumoroid model, we assessed the drug responses of 23 distinct cellular configurations of tumoroids comprised of OVCAR3 HGSC cells, mesenchymal stem cells, HUVEC endothelial cells, and U937 monocytes to an assortment of five therapeutic agents, including carboplatin and paclitaxel. We identified that the overall pooled viability in response to these five drugs was highest among tumoroid compositions that contained a large number of myeloid cells, whereas the most sensitive tumoroids to these agents were comprised of only cancer cells. Additionally, we found that the "mesenchymal tumoroids" containing 400 or more mesenchymal stem cells were more sensitive to carboplatin than paclitaxel. By amalgamating our experimental findings with random forest machine learning algorithms, we assessed the influence of TME cellular composition on treatment reactions. Our findings reveal notable disparities in drug responses correlated with tumoroid composition, underscoring the significance of cellular diversity within the TME as a predictor of therapeutic outcomes. This research establishes a foundation for employing human tumoroids with varied cellular composition as a method to delve into the roles of stromal, immune, and other TME cell types in enhancing cancer cell susceptibility to various treatments.

Most ovarian cancer patients are treated with a standard non-personalized treatment regimen of neoadjuvant chemotherapy comprising platinum and taxane therapy followed by surgical debulking[1]. While this treatment regimen is often initially effective, most patients experience relapse with the development of chemoresistance, leading to high mortality[2,3]. Personalized medicine is a promising approach to improve patient outcomes wherein clinical management is based on the specific characteristics of each individual tumor and patient. However, high-grade serous ovarian cancer (HGSC) has a highly heterogeneous clinical response and a paucity of prognostic factors with which patients can be stratified. Factors like *BRCA1/2* or *CCNE1* mutations can aid in directing clinical management, but ovarian cancer patients are still plagued by frequent development of drug-resistant disease[4,5]. As a result, there has been a considerable effort to define molecular subtypes of HGSC in order to improve prognosis predictions, and more effectively determine the clinical management course of action to improve outcomes[6–11].

In this quest, a seminal study identified four molecular subtypes of HGSC (mesenchymal, immunoreactive, proliferative, and differentiated) in

[1]Department of Biomedical Engineering, University of Michigan, Ann Arbor, MI, USA. [2]Department of Materials Science and Engineering, University of Michigan, Ann Arbor, MI, USA. [3]Macromolecular Science and Engineering, University of Michigan, Ann Arbor, MI, USA. [4]Rogel Cancer Center, University of Michigan, Ann Arbor, MI, USA. [5]AI & Digital Health Innovation, University of Michigan, Ann Arbor, MI, USA. e-mail: mehtagee@umich.edu

microarray analysis of 285 serous and endometrioid tumors[10]. The "mesenchymal" subtype with high stromal and low immune signature corresponded with the worst clinical outcomes, while high immune and differentiated signatures were associated with more favorable outcomes[10]. Since the publication of this report, over the years, these molecular subtypes have been validated by some studies, while others have developed unique molecular classifications of HGSC into similar, yet different subtypes[6–12]. Additionally, single-cell RNA sequencing studies have identified common cell populations in the tumor microenvironment (TME), including fibroblasts, mesenchymal stem cells (MSCs), macrophages, other immune cells, and endothelial cells[13–15]. These studies have suggested that the molecular subtypes are influenced by the proportion of these other non-tumor cell populations within the tumor[14,15]. However, the HGSC molecular subtyping has not been implemented clinically, in part because the specific subtype markers are not statistically significant across all studies[3]. Yet, the promise of using molecular subtyping in HGSC has been demonstrated, for example, in a retrospective study of the effectiveness of anti-angiogenic therapy bevacizumab[16]. By molecular subtyping HGSC, bevacizumab conferred a greater overall benefit in the two subtypes with the worst prognosis (mesenchymal and proliferative), thereby indicating that subtype-specific treatments may improve clinical outcomes[16]. This example highlights the potential of molecular subtype signatures to direct clinical management. Additionally, carcinoma-associated fibroblasts and MSC (CA-MSC)[17–19] and macrophages[20–26] have been shown to influence ovarian cancer cells to adopt more cancer stem-like cell (CSC) phenotypes, become more resistant to chemotherapeutic agents, and become more metastatic. Endothelial cells have been observed to induce cancer stem cell phenotypes and invasion in other cancer types, including glioblastoma and colorectal[27–29]. A better understanding of the role of the nuanced TME cellular composition (i.e., high stromal, high immune, etc.) in patient drug responses to various drugs could enhance the clinical value of HGSC molecular subtyping efforts. Machine learning models are poised to accomplish this goal and provide additional context for developing new treatments and direct the effective administration of current treatments.

Machine learning models are uniquely suited to elucidate the role of nuanced non-tumoral cellular composition in drug response and chemoresistance due to their ability to identify meaningful patterns in complex multi-dimensional datasets[30–32]. As an example, Yu et al. developed a machine learning model trained on proteomic profiles of 130 ovarian serous carcinoma patients to predict response to platinum therapy using various supervised machine learning algorithms and proposed the key pathways involved in platinum resistance with their bioinformatic approach[33]. In another study, explicit mathematical models with a machine learning framework were combined in order to identify candidate combinations of existing therapies and test mechanistic hypotheses for improving treatment efficacy[34]. Together, these and other examples of deep learning and neural network techniques in predicting drug responses highlight the value of interpretable machine learning models in clinical and translational applications[35–40].

Random forest is one of the types of machine learning approaches with high interpretability for biological applications[30,32,41–43]. This approach not only achieves accurate predictions, but is also robust for non-parametric data, outliers, and over-fitting[44]. Furthermore, random forest enables measurement of feature importance to gain information on the process used to generate the model, or what the model "learned" about the data. Therefore, random forest models are a popular choice in biomedical machine learning due to these advantages and have resulted in many successful models[45].

In order to address the unmet need for improved molecular subtyping in HGSC and to clarify the role of the TME cellular composition in response to treatment, we utilized a combination of in vitro drug screening of heterogeneous tumoroids and easily interpretable machine learning techniques in this report. Each of the cell types included in the tumoroids (MSC, endothelial cell, monocyte) has been previously identified to contribute to different molecular subtype signatures[13–15]. Therefore, we created tumoroids of different compositions, where some were predominated by one non-tumor cell type and others contained high proportions of multiple cell types in order to identify the contributions of an individual cell type and the contributions of multiple cell types at the same time. We hypothesize that tumoroids engineered with different cellular compositions (all including tumor cells) will respond differentially to drug treatments. Furthermore, we expect the cell composition of each tumoroid to be used to make predictions of drug response and to gain insights into key cell–cell relationships in evolving chemoresistance. Finally, we expect that the findings from the integrated tumoroid and machine learning model presented in this report will translate to effective molecular subtyping of patient-specific drug responses, in order to improve HGSC response and cure rates.

## Results

### Tumoroids derived from different tumor microenvironment cell compositions respond differentially to 5 different chemo- and targeted therapies

HGSCs are comprised of multiple cell types, including epithelial cancer cells, mesenchymal cancer cells, carcinoma-associated MSCs, microvascular endothelial cells, and macrophages, each of which supports tumor cells in different contexts[14,46,47]. The mesenchymal subtype signature is strongly expressed by the fibroblasts and MSCs, while the immunoreactive signature features myeloid, T cells, and NK cells. Meanwhile, epithelial cells highly express a differentiated signature and, to a lesser extent, express a proliferative signature[48]. In order to investigate the impact of non-tumoral cellular composition on the HGSC chemosensitivity, 23 tumoroids of different cell compositions (Fig. 1A–C, Table 1) were fabricated. Differential morphologies of tumoroids were observed for each of the 23 compositions (Fig. 1C). The responses of cancer cells in tumoroids to conventional chemotherapies (carboplatin and paclitaxel) as well as targeted biologic treatments (PACMA31, N773, and SC144) were tested (Fig. 2A–F) and assessed for viability using the MTS assay following 48 h of drug treatment. Three biologic targeted treatments utilized in this study were: protein disulfide isomerase inhibitor, PACMA31[49]; IL-6/STAT3 inhibitor, SC144[23,50,51]; and E2F/RUNX2 inhibitor (compound N773).

Within each drug treatment, there were significant differences in cancer cell viability between tumoroid cell compositions (Fig. 2A–G). In tumoroids treated with carboplatin, the lowest viability was found in compositions 1 and 3, which were solely composed of OVCAR3 cells, with $0.563 \pm 0.027$ and $0.580 \pm 0.031$ mean normalized viability ± standard error of the mean, respectively. The tumoroids with the highest viability in response to carboplatin were compositions 11 and 21, with $0.954 \pm 0.021$ and $0.887 \pm 0.035$ normalized viability, respectively, which both contained 500 U937s. Similarly, compositions 1 and 3 had the lowest viability of all the tumoroid compositions when treated with paclitaxel ($0.782 \pm 0.016$ and $0.781 \pm 0.023$, respectively), PACMA31 ($0.517 \pm 0.012$ and $0.568 \pm 0.021$, respectively), or N773 ($0.641 \pm 0.018$ and $0.680 \pm 0.012$). However, the tumoroid compositions with the highest viability varied between drug treatments. For paclitaxel, the highest viability was found in tumoroid compositions 14 and 5 ($1.04 \pm 0.025$ and $1.01 \pm 0.023$, respectively), which both contained all four cell types. For PACMA31, the highest viability was found in tumoroid compositions 11 and 7 ($0.956 \pm 0.021$ and $0.900 \pm 0.029$, respectively), which both contained U937s. For N773, the highest viability was found in tumoroid compositions 14 and 11 ($1.00 \pm 0.039$ and $0.976 \pm 0.037$), which both contained U937s. Finally, SC144 deviated the most from the other drugs, with the lowest viability being recorded in tumoroid compositions 20 and 10 ($0.786 \pm 0.029$ and $0.865 \pm 0.030$), which both contained 500 human umbilical vein endothelial cells (HUVECs) and the highest viability in tumoroid compositions 15 and 1 ($1.06 \pm 0.026$ and $1.04 \pm 0.035$), which were quite different from each other in terms of cell composition. ANOVAs were performed to compare viability across tumoroid compositions for each drug treatment, and $p$ values were reported in a heatmap (Fig. 2G). In Fig. 2G, the most significant differences were clustered in the left half of the heatmap, corresponding to comparisons of compositions 1, 2, and 3 (the cancer cell-only conditions) with the other 20

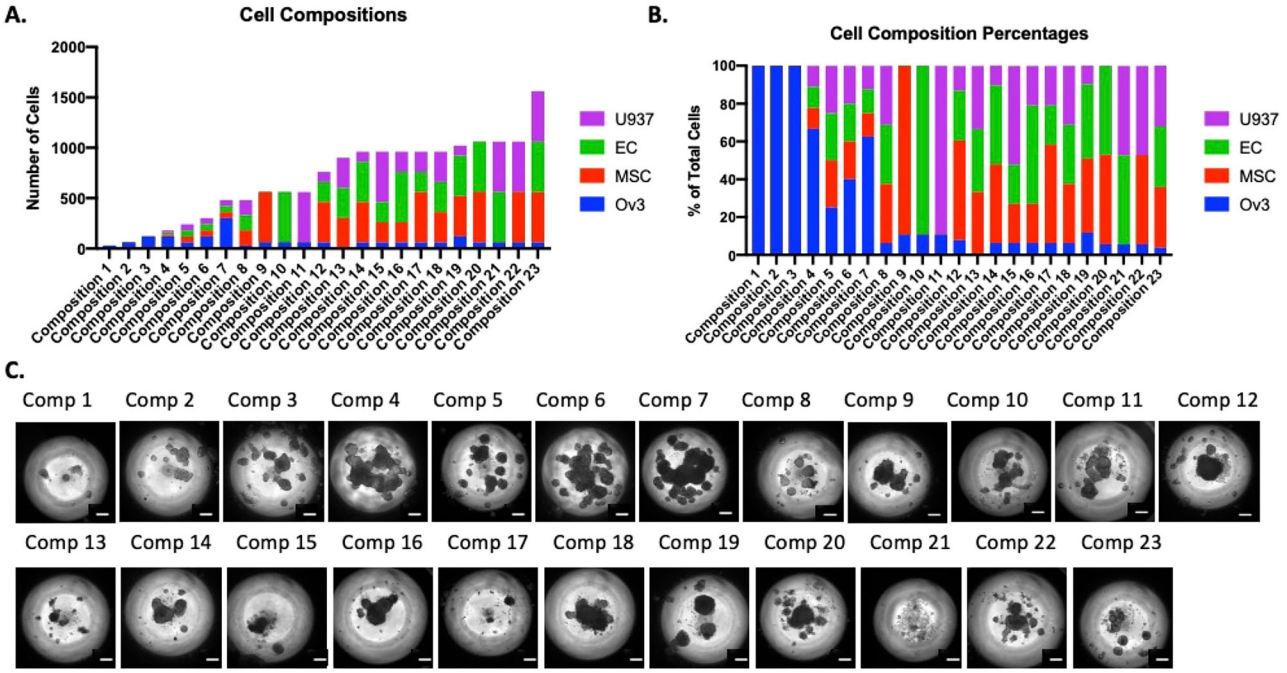


**Fig. 1 | Heterogeneous high-grade serous ovarian tumoroids were created with 23 different cell compositions. A** Bar graph showing the total cell number in each tumoroid composition distributed between high-grade serous cell line OVCAR3 (blue), mesenchymal stem cells (MSCs) (red), endothelial cells (ECs) (green), and U937 monocytes (purple). **B** Bar graph showing the percentage of each cell type in each composition, with OVCAR3 represented in blue, MSCs in red, ECs in green, and U937 monocytes in purple. **C** Phase contrast image of tumoroids taken on day 5, made with each cell composition showing heterogeneous size and morphology. Scale bar = 200 μm.

compositions that also contained non-tumor cells. Paclitaxel, PACMA31, and N773 treatment yielded the most significant differences in viability. Interestingly, a similar cluster of significant differences exists in both the carboplatin and PACMA31 treatment groups (Fig. 2G). Upon examination, these clusters correspond to the increased chemoresistance of composition 11 (with macrophages and cancer cells) compared to compositions 12–20, comprising three or four cell types (all contain MSCs and endothelial cells) (see Fig. 1A, B, Table 1).

We characterized the chemoresistant tumoroids as those with the highest average pooled viability after drug treatments. Notably, the top five chemoresistant tumoroid compositions were compositions 11, 15, 5, 22, and 23 in order of most viable to least, with overall viability of 0.961 ± 0.012, 0.932 ± 0.012, 0.927 ± 0.013, 0.918 ± 0.0099, and 0.911 ± 0.0088, respectively (mean normalized viability ± SEM) (Table 2). Interestingly, four out of the five most resistant compositions on average included 500 U937 (myeloid cells). Similarly, we characterized the chemosensitive tumoroids as those with the lowest average pooled viability after drug treatments. The most chemosensitive tumoroids after all drug treatments were compositions 19, 8, 2, 1, and 3 in order of most viable to least, with overall viability of 0.837 ± 0.016, 0.792 ± 0.0095, 0.788 ± 0.0072, 0.709 ± 0.015, and 0.698 ± 0.012, respectively (Table 3). We noted that the three most sensitive tumoroid compositions, on average, were the only three conditions generated with cancer cells only.

However, the compositions with the greatest resistance and sensitivity to treatment varied depending on the treatment (Tables 2 and 3). Briefly, compositions 11, 21, 22, 5, and 13 were the most resistant to carboplatin treatment, while compositions 19, 7, 14, 3, and 1 were the most sensitive to carboplatin. Notably, composition 13 contained no cancer cells. Contrarily, the most resistant compositions to paclitaxel were compositions 14, 5, 10, 16, and 15, two of which contained 500 ECs (Table 2). Compositions 4, 8, 2, 1, and 3 were the most sensitive to paclitaxel, again including the three tumoroids comprised of cancer cells only. PACMA31 was least effective against and saw the most resistance from compositions 11, 7, 4, 5, and 15. Compositions 18, 8, 2, 3, and 1 were the most sensitive to PACMA31 treatment. Compositions 14, 11, 16, 15, and 22 were most resistant to N773 treatment, including three conditions with 500 U937(myeloid cells). Compositions 19, 8, 2, 3, and 1 were the most sensitive to N773 treatment. Finally, compositions 15, 1, 2, 12, and 7 were most resistant to SC144 treatment. Compositions 19, 23, 3, 10, and 20 were most sensitive to SC144. Interestingly, among the least impacted compositions for SC144 were cancer cell-only compositions with 30 and 60 OVCAR3 cells, respectively (Table 3). Therefore, we observed differential responses to both chemo- and targeted therapies in the 23 tumoroid compositions, with 3 cancer cell-only compositions being the most sensitive to drug treatments. These data highlight the potential clinical application of tumoroids in predicting responses to targeted therapies.

Additionally, these five therapeutic compounds were evaluated on tumoroids generated with CSCs in order to investigate the impact of the stem-like cell status of the cancer cells on the drug response. OVCAR3 cells were sorted using FACS for $ALDH^+$ and $CD133^+$ cells to obtain CSCs. These CSCs were then incorporated into tumoroids in place of the bulk OVCAR3 cells. A few tumoroid compositions (2, 9, 10, and 20) were generated using CSCs and treated with carboplatin, paclitaxel, SC144, N773, and PACMA31 (Supplementary Fig. S1). The tumoroids, which included non-tumor cells, tended to be more resistant to these agents compared to cancer cell-only tumoroids, even when all the tumoroids were generated with CSCs.

### "Mesenchymal" tumoroids respond differentially to carboplatin and paclitaxel

Reports in the literature support that "mesenchymal" subtypes are more sensitive to taxane (paclitaxel) therapy and more resistant to platinum-based therapies[52]. "Mesenchymal" subtype signatures have also been linked to the presence of mesenchymal cells, as opposed to more mesenchymal cancer cell populations[14]. Therefore, in order to draw a first pass clinical parallel with our tumoroid models, we compared the drug response of 7 "mesenchymal tumoroid" compositions (compositions 9, 12, 14, 17, 20, 22, and 23) characterized by ≥400 MSCs, to carboplatin treatment versus

**Table 1 | The tumoroid cell compositions are listed with the number of cancer cells, mesenchymal stem cells, endothelial cells, and monocytes in each of the 23 experimental conditions**

| | Cancer cells (OVCAR3) | Mesenchymal stem cells (MSC) | Endothelial cells (HUVEC) | Monocytes (U937) |
|---|---|---|---|---|
| Composition 1 | 30 | 0 | 0 | 0 |
| Composition 2 | 60 | 0 | 0 | 0 |
| Composition 3 | 120 | 0 | 0 | 0 |
| Composition 4 | 120 | 20 | 20 | 20 |
| Composition 5 | 60 | 60 | 60 | 60 |
| Composition 6 | 120 | 60 | 60 | 60 |
| Composition 7 | 300 | 60 | 60 | 60 |
| Composition 8 | 30 | 150 | 150 | 150 |
| Composition 9 | 60 | 500 | 0 | 0 |
| Composition 10 | 60 | 0 | 500 | 0 |
| Composition 11 | 60 | 0 | 0 | 500 |
| Composition 12 | 60 | 400 | 200 | 100 |
| Composition 13 | 0 | 300 | 300 | 300 |
| Composition 14 | 60 | 400 | 400 | 100 |
| Composition 15 | 60 | 200 | 200 | 500 |
| Composition 16 | 60 | 200 | 500 | 200 |
| Composition 17 | 60 | 500 | 200 | 200 |
| Composition 18 | 60 | 300 | 300 | 300 |
| Composition 19 | 120 | 400 | 400 | 100 |
| Composition 20 | 60 | 500 | 500 | 0 |
| Composition 21 | 60 | 0 | 500 | 500 |
| Composition 22 | 60 | 500 | 0 | 500 |
| Composition 23 | 60 | 500 | 500 | 500 |

paclitaxel treatment (Fig. 3A–G). This comparison yielded the opposite relationship than expected from literature, with carboplatin being more effective in each of the selected "mesenchymal tumoroids" (0.703, 0.704, 0.623, 0.698, 0.761, 0.858, and 0.792 normalized viability, respectively) compared to paclitaxel treatment (0.920, 0.994, 1.04, 0.964, 0.967, 0.945, and 0.984 normalized viability, respectively). These differences in paclitaxel versus carboplatin response were significantly different, with unpaired *t*-tests revealing *p* values of <0.0001, <0.0001, <0.0001, <0.0001, <0.0001, 0.0161, and <0.0001 for compositions 9, 12, 14, 17, 20, 22, and 23, respectively.

To combat the relative effectiveness of carboplatin versus paclitaxel dosing, we next examined the relative ranking of the "mesenchymal tumoroids" compared to all other compositions treated with carboplatin or paclitaxel (Fig. 3H). We expected that "mesenchymal tumoroids" would rank in the most resistant compositions among the carboplatin treatment group and in the least resistant compositions among the paclitaxel treatment group. Surprisingly, the tumoroids with the most MSC were more sensitive to carboplatin, with an average ranking of 12.7 (in the bottom half of all compositions), while the "mesenchymal tumoroids" were more resistant to paclitaxel, with an average rank of 8.6 (in the top half of all compositions). Additionally, the most resistant composition to paclitaxel, composition 14, is a "mesenchymal tumoroid." Of note, composition 22 was the only "mesenchymal tumoroid" that showed the expected trend (third most resistant composition to carboplatin and the thirteenth most resistant to paclitaxel). We also noted that the composition without cancer cells, composition 13, also followed the expected "mesenchymal" subtype trend, being the fifth most resistant to carboplatin and the fifteenth most resistant to paclitaxel. Therefore, the "mesenchymal tumoroids" with higher numbers of MSCs were sensitive to carboplatin and resistant to paclitaxel, which is opposite to the literature report for "mesenchymal" subtype signature.

### Machine learning models predicted drug responses based on the tumoroid cellular composition

To investigate the utility of the TME cell composition in predicting treatment response, random forest models were created to predict tumoroid response to each drug based on cell composition. The primary purpose of the machine learning approach was to use it as a tool to establish potential relationships between cell composition features and response to drug treatment, not necessarily to generate highly accurate prediction models. The median normalized absorbance value from the MTS viability assays for each drug treatment was used to determine "high" or "low" response to the drug.

The random forests had variable effectiveness at predicting response to different drugs. The worst model (predicting SC144 response) had an area under the curve (AUC) of 0.5883 for the training set and 0.6264 for the test set (Fig. 4E). Contrarily, the most effective random forest model had an AUC of 0.6915 for the training set and an AUC of 0.6832 on the test set when trained to predict PACMA31 response (Fig. 4C). Paclitaxel (training AUC: 0.6825; test AUC: 0.6898; Fig. 3B) and N773 (training AUC: 0.6415; test AUC: 0.6833; Fig. 4D) predictions were the second and third most accurate. The carboplatin model was the second-to-last most effective with a training AUC of 0.6089 and a test AUC of 0.6695 (Fig. 4A). Each model performed better than a random predictor and was relatively consistent between the training and test sets, indicating a lack of overfitting. Training set AUCs ranged from 0.5883 to 0.6915, indicating moderate performance. Interestingly, the three most accurate prediction models (PACMA31, paclitaxel, and N773) were based on treatments with the greatest significant difference in viability between experimental conditions with and without non-tumoral cells (Fig. 2G).

### Random forest models predicted the most important parameters for individual drug response

We evaluated the importance of each tumoroid composition parameter in making predictions for each drug response. None of the random forest models prioritized the number of a single cell type in making predictions. The carboplatin model placed relatively equivalent importance on most of its parameters, but still put the most weight on the proportion of the tumoroid made up of U937 (myeloid cells). The proportion of the tumoroid made up of endothelial and MSCs respectively were also in the top 5 most important parameters in the carboplatin model (Fig. 5A). The paclitaxel response predictor placed the most importance by far on the total number of cells and the total number of all tumor and non-tumor cells plated at the start of experiment (Fig. 5B). As the total number of TME cells is highly influential in the total number of cells (more non-tumoral cells inherently means more total cells), these two parameters are heavily overlapping. PACMA31 predictions placed the most importance on the ratio of cancer cells to TME cells and to total cells, respectively (Fig. 5C). The N773 model placed a similar weight on the ratio of cancer cells to total cells and the total number of cells alone. Finally, the SC144 model placed the greatest importance on the cancer cell type (OVCAR3 sorted for CSCs markers[19,23,53,54] ALDH and CD133, compared to unsorted OVCAR3), as an experiment was conducted with sorted ovarian CSCs as opposed to unsorted OVCAR3. The SC144 model also placed high importance on the proportion of myeloid cells in the tumoroids (Fig. 5E). Figure 5F shows a heatmap of the importance value of each parameter for each drug response prediction model, revealing a clear pattern of the importance with the proportion of cancer cells and TME cells in each tumoroid being critical parameters. The heatmap also reveals moderate importance placed on various cell–cell relationships, whereas the parameters that considered only individual cell type numbers were among the least important for all models.

Breaking down the most important parameters for each model and plotting the important parameter versus the treatment response showed the relationship between each tumoroid composition variable and the

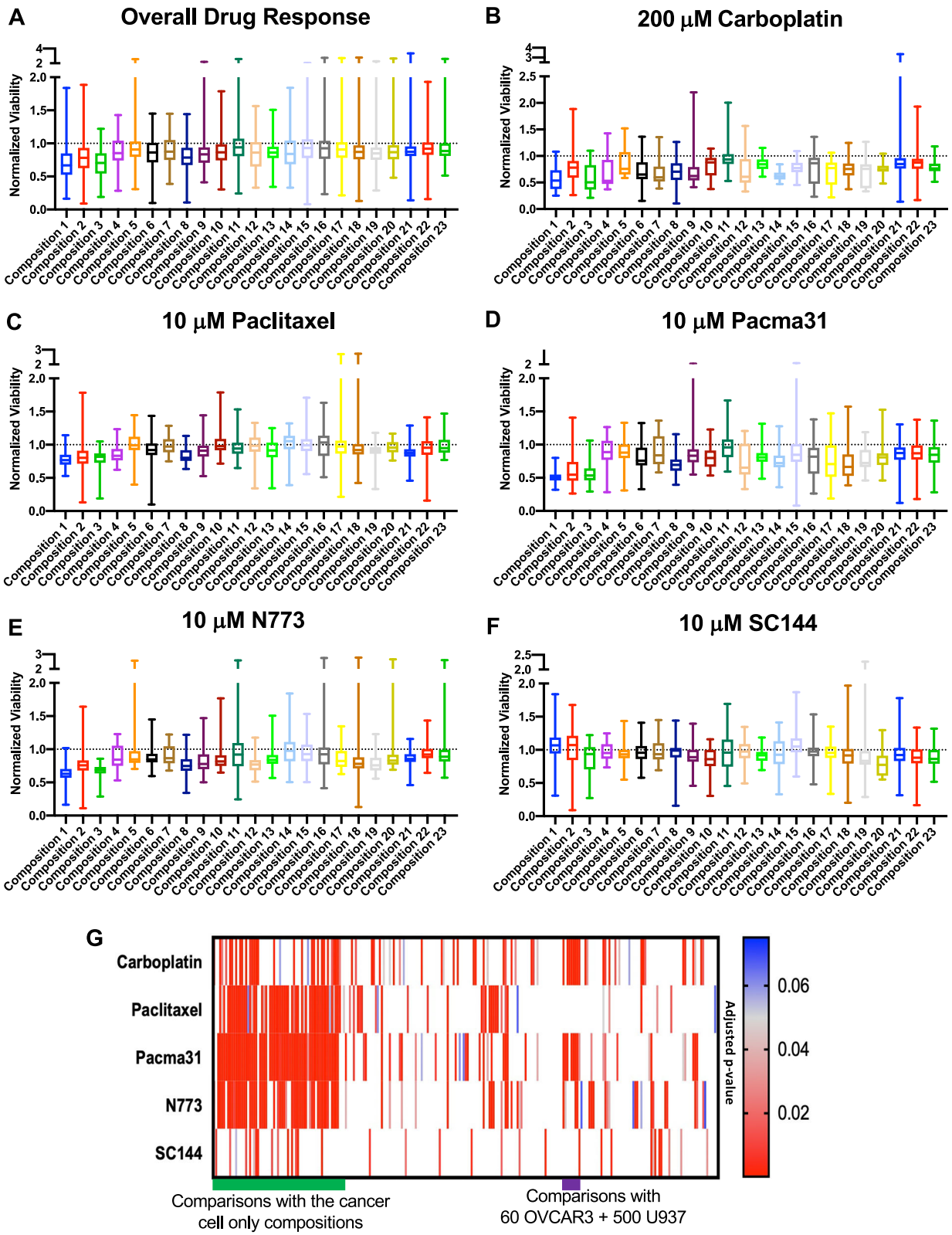


**Fig. 2 | Heterogeneous high-grade serous ovarian tumoroids with different cell compositions have statistically significant differences in drug treatment response. A** Box and whisker plot of averaged normalized viability for each tumoroid cell composition across all treatment conditions, showing overall resistance to treatment. Box and whisker plots showing resistance of each tumoroid composition to **B** carboplatin, **(C)** paclitaxel, **(D)** PACMA31, **(E)** N773, and **F** SC144. **G** Heatmap of adjusted *p* values for comparisons between all conditions determined via one-way ANOVA and Tukey's post hoc analysis. Red indicates most significant ($p < 0.05$), gray indicates borderline significance ($p = 0.05$), and blue and white indicate not significant ($p > 0.05$).

https://doi.org/10.1038/s44385-025-00032-y



**Table 2 | The top 5 most resistant tumoroid compositions for each treatment are listed with their corresponding normalized viability values**

| | Most resistant tumoroid cellular composition for each treatment | | | | | |
|---|---|---|---|---|---|---|
| **Order of resistance** | **Overall drug response** | **Carboplatin drug response** | **Paclitaxel drug response** | **PACMA31 drug response** | **N773 drug response** | **SC144 drug response** |
| 5<br>most resistant | Composition 11<br>*60 OVCAR3 + 500 U937* | Composition 11<br>*60 OVCAR3 + 500 U937* | Composition 14<br>*60 OVCAR3 + 400 MSC + 400 EC + 100 U937* | Composition 11<br>*60 OVCAR3 + 500 U937* | Composition 14<br>*60 OVCAR3 + 400 MSC + 400 EC + 100 U937* | Composition 15<br>*60 OVCAR3 + 200 MSC + 200 EC + 500 U937* |
| 4 | Composition 15<br>*60 OVCAR3 + 200 MSC + 200 EC + 500 U937* | Composition 21<br>*60 OVCAR3 + 500 EC + 500 U937* | Composition 5<br>*60 OVCAR3 + 60 MSC + 60 EC + 60 U937* | Composition 7<br>*300 OVCAR3 + 60 MSC + 60 EC + 60 U937* | Composition 11<br>*60 OVCAR3 + 500 U937* | Composition 1<br>*30 OVCAR3* |
| 3 | Composition 5<br>*60 OVCAR3 + 60 MSC + 60 EC + 60 U937* | Composition 22<br>*60 OVCAR3 + 500 MSC + 500 U937* | Composition 10<br>*60 OVCAR3 + 500 EC* | Composition 4<br>*120 OVCAR3 + 20 MSC + 20 EC + 20 U937* | Composition 16<br>*60 OVCAR3 + 200 MSC + 500 EC + 200 U937* | Composition 2<br>*60 OVCAR3* |
| 2 | Composition 22<br>*60 OVCAR3 + 500 MSC + 500 U937* | Composition 5<br>*60 OVCAR3 + 60 MSC + 60 EC + 60 U937* | Composition 16<br>*60 OVCAR3 + 200 MSC + 500 EC + 200 U937* | Composition 5<br>*60 OVCAR3 + 60 MSC + 60 EC + 60 U937* | Composition 15<br>*60 OVCAR3 + 200 MSC + 200 EC + 500 U937* | Composition 12<br>*60 OVCAR3 + 400 MSC + 200 EC + 100 U937* |
| 1<br>least resistant | Composition 23<br>*60 OVCAR3 + 500 MSC + 500 EC + 500 U937* | Composition 13<br>*300 MSC + 300 EC + 300 U937* | Composition 15<br>*60 OVCAR3 + 200 MSC + 200 EC + 500 U937* | Composition 15<br>*60 OVCAR3 + 200 MSC + 200 EC + 500 U937* | Composition 22<br>*60 OVCAR3 + 500 MSC + 500 U937* | Composition 7<br>*300 OVCAR3 + 60 MSC + 60 EC + 60 U937* |

**Table 3 | The top 5 most sensitive tumoroid compositions for each treatment are listed with their corresponding normalized viability values**

| | Most sensitive tumoroid cellular composition for each treatment | | | | | |
|---|---|---|---|---|---|---|
| **Order of sensitivity** | **Overall drug response** | **Carboplatin drug response** | **Paclitaxel drug response** | **PACMA31 drug response** | **N773 drug response** | **SC144 drug response** |
| 5<br>least sensitive | Composition 19<br>*120 OVCAR3 + 400 MSC + 400 EC + 100 U937* | Composition 19<br>*120 OVCAR3 + 400 MSC + 400 EC + 100 U937* | Composition 4<br>*120 OVCAR3 + 20 MSC + 20 EC + 20 U937* | Composition 18<br>*60 OVCAR3 + 300 MSC + 300 EC + 300 U937* | Composition 19<br>*120 OVCAR3 + 400 MSC + 400 EC + 100 U937* | Composition 19<br>*120 OVCAR3 + 400 MSC + 400 EC + 100 U937* |
| 4 | Composition 8<br>*30 OVCAR3 + 150 MSC + 150 EC + 150 U937* | Composition 7<br>*300 OVCAR3 + 60 MSC + 60 EC + 60 U937* | Composition 8<br>*30 OVCAR3 + 150 MSC + 150 EC + 150 U937* | Composition 8<br>*30 OVCAR3 + 150 MSC + 150 EC + 150 U937* | Composition 8<br>*30 OVCAR3 + 150 MSC + 150 EC + 150 U937* | Composition 23<br>*60 OVCAR3 + 500 MSC + 500 EC + 500 U937* |
| 3 | Composition 2<br>*60 OVCAR3* | Composition 14<br>*60 OVCAR3 + 400 MSC + 400 EC + 100 U937* | Composition 2<br>*60 OVCAR3* | Composition 2<br>*60 OVCAR3* | Composition 2<br>*60 OVCAR3* | Composition 3<br>*120 OVCAR3* |
| 2 | Composition 1<br>*30 OVCAR3* | Composition 3<br>*120 OVCAR3* | Composition 1<br>*30 OVCAR3* | Composition 3<br>*120 OVCAR3* | Composition 3<br>*120 OVCAR3* | Composition 10<br>*60 OVCAR3 + 500 EC* |
| 1<br>most sensitive | Composition 3<br>*120 OVCAR3* | Composition 1<br>*30 OVCAR3* | Composition 3<br>*120 OVCAR3* | Composition 1<br>*30 OVCAR3* | Composition 1<br>*30 OVCAR3* | Composition 20<br>*60 OVCAR3 + 500 MSC + 500 EC* |

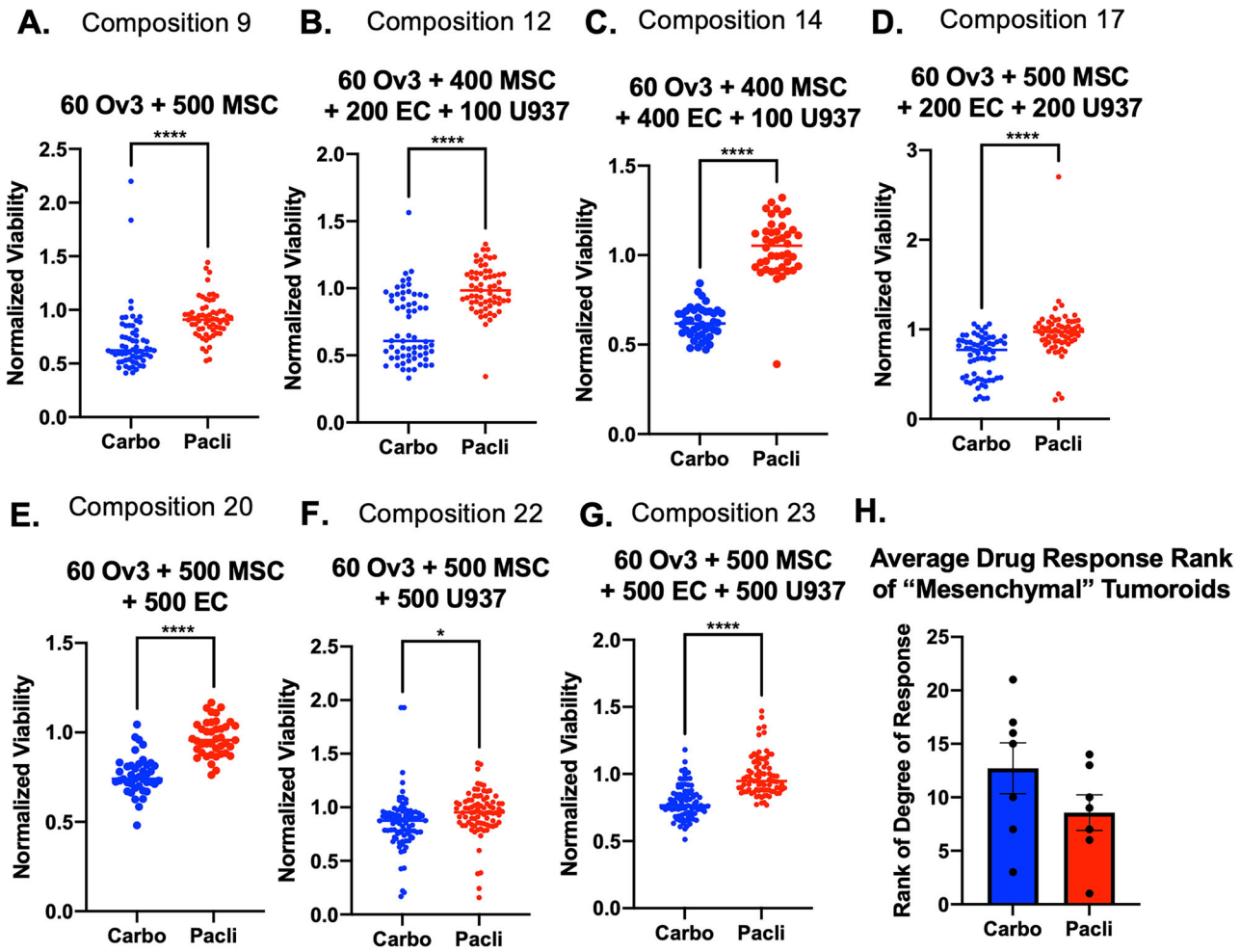


**Fig. 3 | Comparison of carboplatin and paclitaxel response among high-grade serous ovarian tumoroids with the highest number of mesenchymal stem cells, termed "mesenchymal tumoroids".** **A**–**G** Average normalized viability of each mesenchymal tumoroid following treatment with carboplatin or paclitaxel. **H** Average resistance rank of each "mesenchymal tumoroid" to carboplatin (blue) or paclitaxel (red) compared to all other tumoroid compositions. Error bars represent the standard error of the mean. Results of unpaired *t*-tests are represented by $^{*}p \le 0.05$, $^{**}p \le 0.01$, $^{***}p \le 0.001$, $^{****}p \le 0.0001$.

treatment response (Fig. 6A–E). In general, there appears to be an inverse relationship between drug response and the total number of non-tumoral cells, which is highly correlated with the total cell number. For example, PACMA31 appears to be most effective when the ratio of cancer cells to MSCs, endothelial, and myeloid cells is high (i.e., there are no added TME cells) (Fig. 6C). Interestingly, the SC144 prediction model placed the most importance on the type of OVCAR3 cells used, as tumoroids made with CSC-sorted OVCAR3 were more susceptible to SC144. Moreover, when examining the second most important parameter in predicting response to carboplatin, low ratios of OVCAR3 to MSC (a higher proportion of MSC than cancer cells) resulted in generally greater resistance to carboplatin treatment (Fig. 6F). Therefore, the random forest models revealed the most important parameters that were instrumental in predicting the individual drug responses.

## Discussion

The cellular composition of the TME has previously been reported in driving differential treatment responses between HGSC molecular subtypes[14,46,48]. However, there is an incomplete understanding of the role of more nuanced differences in non-tumoral cellular composition on treatment outcomes. In this work, we leveraged a 3D, tunable heterogeneous tumoroid platform to screen the drug responses of tumoroids representing 23 distinct compositions of tumor cells, MSCs, endothelial, and myeloid cells. Screening data was subsequently used to generate random forest models to predict drug response based on tumoroid cell composition.

The most significant differences in treatment response were found between tumoroid compositions with only cancer cells and those with added TME non-tumoral cells. The three most sensitive compositions contained only cancer cells, supporting the role of TME cells in conferring chemoresistance, as expected based on the literature[19,55–57]. Differences in drug response between compositions with varying numbers of TME cells suggest composition-dependent chemoresistance effects. From a clinical application perspective, this indicates the importance of choosing a therapy compatible with the tumor composition. For example, based on the data presented in this study, PACMA31, paclitaxel, and N773 would be relatively less effective in tumors with high stromal content compared to carboplatin or SC144.

Treatments with paclitaxel, PACMA31, and N773 yielded the most significant differences in viability, potentially indicating that their respective mechanisms of action are more attenuated by non-tumor cells than the mechanisms leveraged by carboplatin and SC144. Significant differences were identified in the cluster of tumoroid compositions treated with carboplatin and PACMA31, with increased chemoresistance of composition 11 compared to compositions 12–20. This cluster of differences included the significant difference between composition 11 and composition 15, which both contain 500 myeloid cells, refuting the rationale that myeloid cells are solely responsible for the chemoresistance observed in composition 11. It is possible that carboplatin and PACMA31 are negatively influencing viability

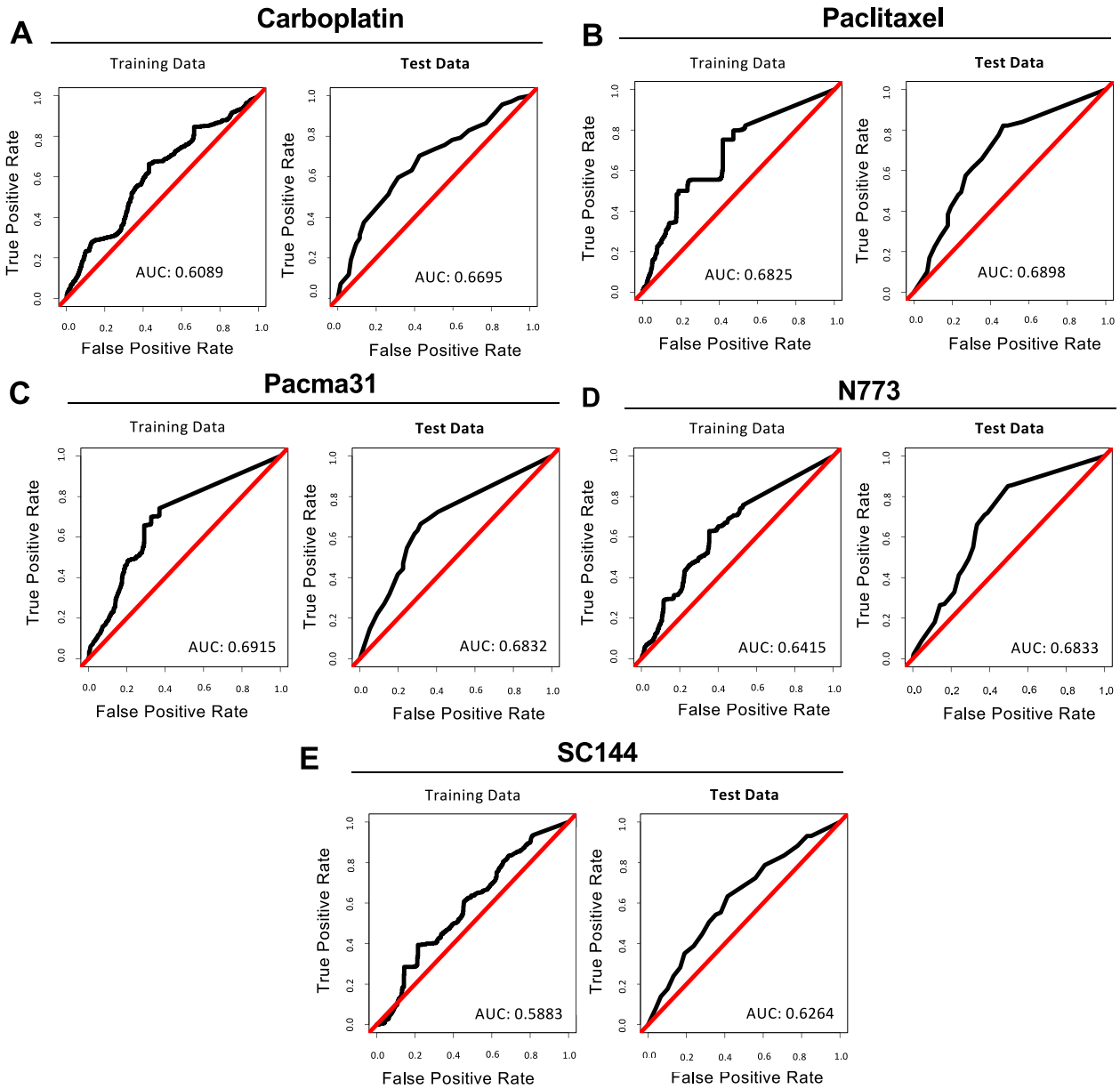


**Fig. 4 | Random forest model performed better than random predictors at predicting drug responses to each treatment for all tumoroid cell compositions.** Receiver operating characteristic curves (ROCs) for the training (left) and test (right) set for the random forest model generated to predict response to **A** carboplatin, **(B)** paclitaxel, **(C)** PACMA31, **(D)** N773, and **E** SC144.

in composition 15 through effects on the MSCs and/or ECs. However, PACMA31 has previously been reported to be effective against ovarian cancer cells and non-toxic to healthy tissues[49]. Alternatively, it is possible that the MSCs and/or ECs are interacting with the cancer cells and/or myeloid cells to attenuate the chemoresistant effect observed in composition 11. The molecular mechanism driving this response requires further experimentation but poses some interesting questions with potential translational implications. We additionally observed that paclitaxel was least effective against compositions 14, 5, 10, 16, and 15, two of which contained 500 ECs, potentially indicating a connection between ECs and resistance to paclitaxel (Table 3). This is contrary to previous reports of anti-angiogenic and endothelial-specific effects of paclitaxel[58–60]. However, it is possible that ECs are conferring chemoresistance through indirect mechanisms such as the modulation of tumoroid extracellular matrix[61].

After generating random forest models for each drug treatment, we found that the model predicting SC144 response had the worst performance but was still better than a random prediction model. The tumoroid compositions that were least impacted by SC144 contained cancer cell-only compositions. SC144 inhibits gp130 through binding, resulting in gp130 phosphorylation and deglycosylation, and ultimately abrogates STAT3 phosphorylation and subsequent downstream gene activation[62]. Through these mechanisms, SC144 was previously shown to be effective against ovarian cancer cell lines in vitro and in vivo[62]. However, in our tumoroid platform, overall response across all conditions was low as indicated by sparse significant differences between experimental compositions. This low overall response perhaps suggests the need for increased doses in our system to identify true responses. More robust drug responses obtained with higher concentration treatment or longer duration treatment could also reduce overlap in response values between compositions, potentially leading to more accurate model predictions. However, STAT3 has been implicated in ovarian CSC maintenance, and therefore, the inhibitor SC144 may be more effective against CSC[63]. We tested this theory on a subset of the tumoroid

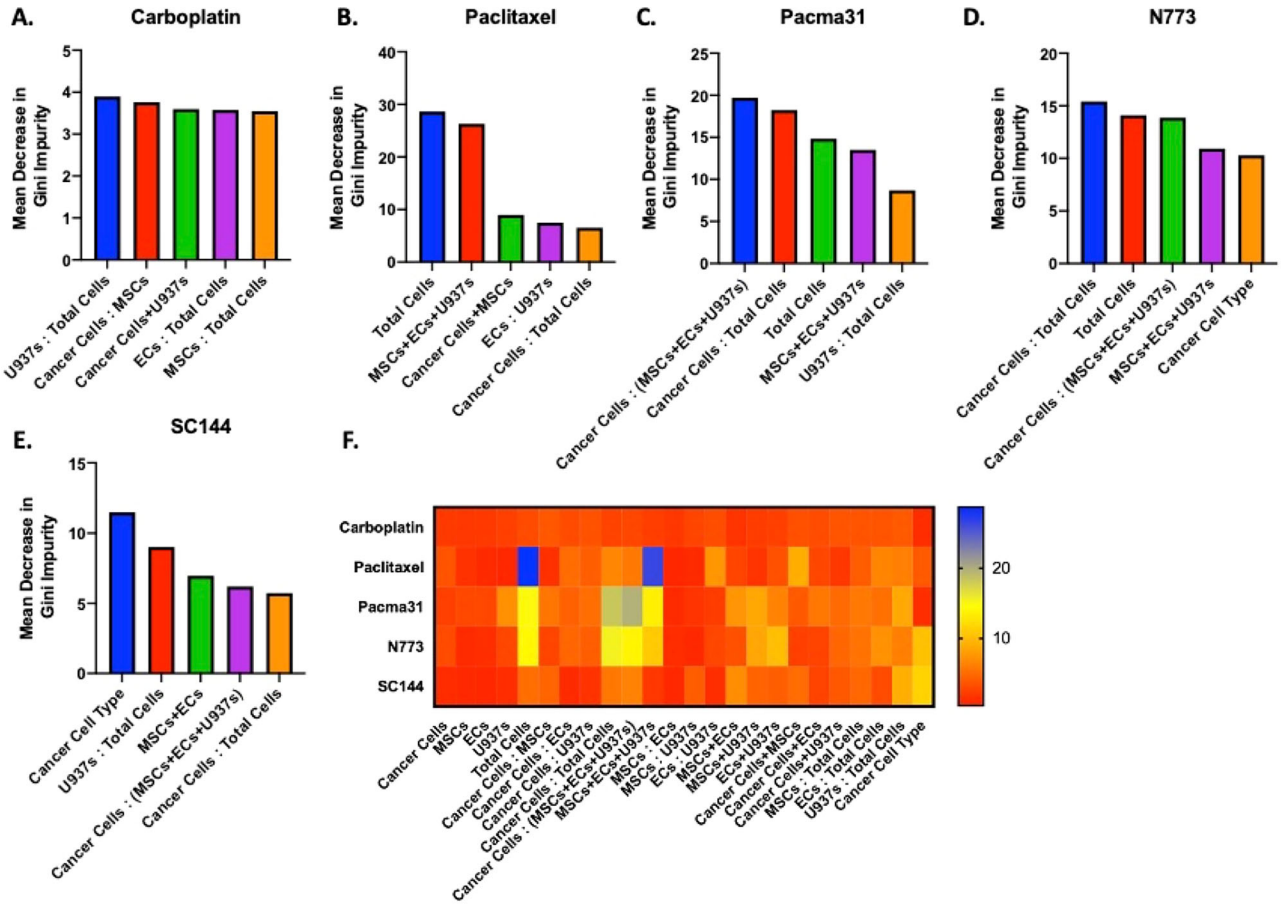


**Fig. 5 | Random forest model provided easily accessible variable importance measures to facilitate interpretation of results.** Top 5 most influential parameters in predicting drug response to **(A)** carboplatin, **(B)** paclitaxel, **(C)** PACMA31, **D** N773, and **E** SC144. **F** Heatmap of the importance measures of all parameters for each drug prediction model across all tumoroid cell compositions.

compositions and indeed found lower viability in response to the same concentration of SC144 in these CSC tumoroids compared to bulk OVCAR3 tumoroids. Therefore, this drug may have a more impactful clinical response in tumors that have high CSC levels. Additionally, our model performance may be improved by testing this drug on more tumoroid compositions, instead of just 4.

When we examined the response of "mesenchymal tumoroids" (those with at least 400 MSCs) to carboplatin and paclitaxel effectiveness, we found that carboplatin was more effective in the selected "mesenchymal" compositions compared to paclitaxel treatment. This was contrary to expectation. Although, like SC144, paclitaxel had a low overall response, suggesting the potential need for higher doses or longer treatments to ensure that treatment effects are not being obscured. This finding could also be due to a number of factors, including the crude nature with which we defined "mesenchymal tumoroids." It is possible that some other tumoroid compositions would be classified as a mesenchymal subtype if they were to be sequenced, even with lower numbers of MSC at the start of the experiment. In fact, previous work in our lab compared the gene expression in patient-specific tumoroids made with composition 18 (60 patient-specific tumor cells + 300 MSC + 300 EC + 300 PBMC) versus matched patient-specific spheroids made with only 60 patient tumor cells. In this work, patient-specific tumoroids were found to be more resistant to carboplatin treatment and to have a transcriptome reflective of the mesenchymal subtype. From this, we may infer that composition 18 in this analysis, and perhaps other compositions, could have been justifiably considered as "mesenchymal tumoroids." However, in the absence of sequencing data to group each composition into appropriate molecular subtypes, this possible explanation remains conjecture. Furthermore, while mesenchymal subtypes have been attributed to the presence of mesenchymal cells, the subtype signature may also be influenced by other cell types in the stroma, making our crude definition of a "mesenchymal tumoroid" less meaningful.

We found that paclitaxel was least effective against compositions 14, 5, 10, 16, and 15, all of which contained 500 ECs. This is not in line with previous reports of anti-angiogenic effects of paclitaxel but might be related to ECs conferring chemoresistance through modulation of tumoroid extracellular matrix. The response to SC144 was low across all conditions, suggesting a need for higher doses. Carboplatin was more effective in "mesenchymal tumoroids" (those with at least 400 MSCs) compared to paclitaxel, which had a low overall response. Only composition 22 was the most representative of the "mesenchymal" molecular subtype. The three most accurate prediction models (PACMA31, paclitaxel, and N773) were those that had the most significant differences in response between cancer cell-only conditions and compositions with added non-tumoral cells, indicating that these three drugs would be less effective in tumors with high stromal content. Overall, training set AUCs ranged from 0.5883 to 0.6915, indicating moderate performance. However these values are in line with those of previous drug prediction models generated based on protein (AUC: ~0.58–0.64 for various machine learning algorithms)[33] or molecular features (AUC: ~0.56–0.76 for a Deep Neural Network model)[64] demonstrating the potential of predictions made based solely on cell composition.

The results of this study highlight the importance of considering complex relationships between cell types in predicting drug response. The random forest models did not use the quantity of a single cell type as a significant factor, but rather more complex parameters that considered multiple cell types. One example was the relationship between PACMA31 response and the ratio of cancer cells to MSCs, ECs, and U937s, where a high

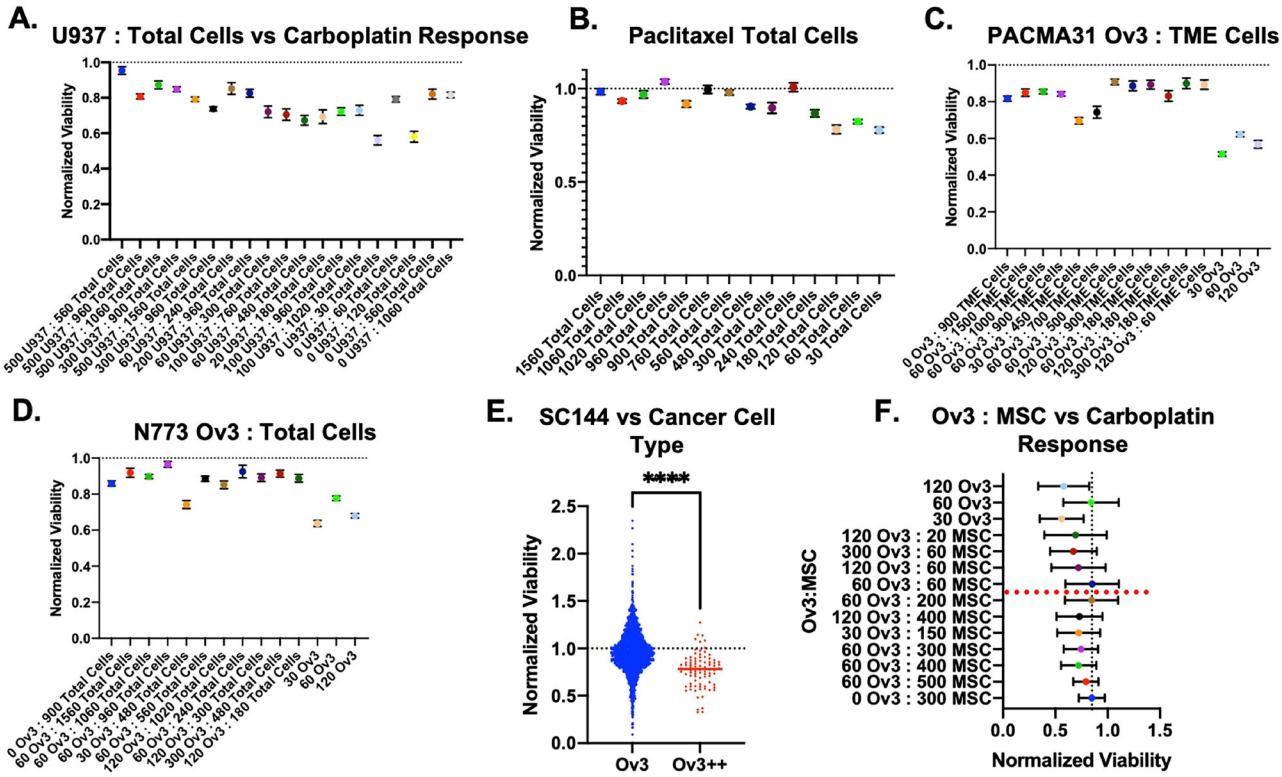


**Fig. 6 | Normalized viability versus the important features for each random forest model reveals cell composition dynamics in drug response prediction.** The most important features in predicting response to **A** carboplatin, **(B)** paclitaxel, **(C)** PACMA31, **(D)** N773, and **E** SC144 versus normalized viability. **F** Plotting the second most important feature in predicting carboplatin response versus normalized viability reveals the expected relationship between the presence of mesenchymal cells and resistance to carboplatin (higher ratios of MSCs to OVCAR3 are associated with greater resistance to carboplatin).

ratio of cancer cells was found to be more effective. Another example was the importance of the type of OVCAR3 cells used in the experiment for predicting SC144 response, where tumoroids made with sorted OVCAR3 CSCs were more susceptible to SC144[65–67], potentially due to SC144's ability to prevent STAT3 activation, which is known to be involved in CSC maintenance. These findings emphasize the need for complex in vitro models with more than two cell types for drug screening applications and the limitations of human observation alone in understanding the nuanced aspects of TME-conferred chemoresistance.

Lastly, examining the relationships between important parameters and drug response showed the direction between each parameter and treatment response. A more nuanced analysis, using the ratio of cancer cells to MSCs, showed the expected carboplatin response trend of increased resistance in more mesenchymal tumors. This highlights the importance of cell–cell relationships in drug response stratification. Machine learning models have the potential to predict therapy response based on cell composition and evaluate the importance of each parameter. Although the models have moderate accuracy, they can be improved with more physiologically relevant tumoroids (with matched cancer-associated stromal and immune cells) and higher concentration or longer duration drug treatments to obtain more robust drug responses.

Recent work has suggested that the stromal cells can impact molecular subtyping classifications and thus may have prognostic significance[14,47,68], however, the exact role of nuanced differences in stromal composition in drug response is still unclear. Furthermore, current drug treatment prediction models rely on bulk-omics measurements or expensive imaging techniques, which are often limited in sample size and only exist for previously administered therapies[32,33,43,69–72], limiting their utility in predicting response to novel therapies. In this work, we developed an in vitro model system to generate tumoroids with different cell compositions and tested drug response using a high-throughput hanging drop plate platform. Random forest models were used to predict drug response based on tumoroid composition. The results showed significant differences in drug response based on tumoroid composition, supporting the importance of the cellular composition of the TME in predicting therapy response[18,19,29,73–75]. Yet, it highlights the importance of nuanced differences in cell composition that may obscure the drug responses. This work provides proof of concept for using tumoroids with different compositions to investigate the role of TME cells in resistance to therapies.

## Methods

### Cell culture and materials

Epithelial ovarian cancer cells (OVCAR3: American Type Culture Collection, ATCC) were cultured in RPMI 1640 (Gibco) supplemented with 10% fetal bovine serum (FBS: Atlanta Biologics) and 1% antibiotics and antimycotics. Human adipose-derived MSCs (haMSCs: Lonza PT-5006) were cultured in Adipose-derived Stem Cell Basal Medium (Lonza) supplemented with 10% FBS and 1% antibiotics and antimycotics as well as 2 mM L-glutamine (Gibco). HUVECs were a donation from Lonza and were cultured in Endothelial Basal Medium-2 (EBM-2 [AKA EGM-2]: Lonza). U937 monocytes were purchased from ATCC and were cultured in 1640 RPMI supplemented with 10% heat-inactivated FBS and 1% antibiotics and antimycotics. Tumoroid cultures were formed in 384-well hanging drop plates in Tumoroid Medium (TM) (2X SFM: EBM-2 (5:1) + 20 μM ROCK inhibitor). See Supplementary Table S1 for detailed composition.

### Cancer stem-like cell (CSC) isolation

Ovarian CSCs were isolated from the HGSC cell line OVCAR3 as described previously[76]. Briefly, cells were harvested and incubated with ALDEFLUOR reagent (Stem Cell Technologies, Vancouver, BC), and CD133 antibody (Milentyi Biotech, San Diego, CA), and sorted using flow cytometry for cells positive for elevated ALDH and CD133 positivity. Appropriate DEAB and

isotype controls were used for both assays to determine gate settings as described previously[77,78]. CSCs were freshly sorted and used to make tumoroids within <24 h after flow sorting.

### Tumoroid fabrication in hanging drop plates

To plate tumoroids in 384-well hanging drop plates, each cell type is collected from 2D plates and resuspended in its respective 2D culture medium for counting on a hemacytometer. The cell density of each cell type is calculated and then used to calculate the total volume of that cell suspension that will be needed to obtain the required number of that cell type for each experimental composition. The calculated volume of each cell suspension is then added into a single tube per tumoroid composition, spun down at 800 × *g*, and resuspended in the appropriate volume of tumoroid medium so that every well plated on the hanging drop plate will receive 20 μL of the desired number of each cell type.

### Maintenance and drug treatment of tumoroids

Tumoroids were imaged on days 3, 5, and 7 using an epifluorescent Olympus microscope to obtain phase contrast images (4×). On day 3, tumoroids are supplemented with 2 μL of tumoroid medium per well. On day 5, each tumoroid composition was fed with 2 μL of tumoroid medium with no drug as a control or 200 μM carboplatin, 10 μM paclitaxel, 10 μM PACMA31, 10 μM N773, and 10 μM SC144. Each treatment condition contained 20–40 wells as technical replicates. Plates were incubated for 48 h and imaged on day 7.

### Tumoroid viability

To quantify viability, an MTS assay was used. Two microliters of MTS reagent were added to each well, and plates were incubated at 37 °C. Absorbance was then measured in each well at 2- and 4-h incubation time points. Normalized viability was quantified by averaging all control wells and dividing the absorbance in each well by the control average to obtain viability measurements for each drug in reference to the viability of the control. Drug assays for each tumoroid composition were repeated in 2–12 separate experiments (most compositions were 2–4 replicates, but compositions 2 and 18 had 12 and 7 replicates each because they served as frequent control compositions).

### Data processing

Normalized MTS viability data were compiled into an Excel spreadsheet and coupled with the corresponding input cell composition for a given experiment. To avoid "zero values" that would lead to "N/As" that need to be excluded or imputed in random forest models, a value of 0.001 was added to all cell numbers. Features were generated by calculating various relationships between the four cell numbers obtained at the inception of the experiment. These included the following and are shown in Supplementary Table S2: (Cancer cells, haMSCs, HUVECs, U937s, Total cells, Cancer cells: haMSC, Cancer cells: HUVECs, Cancer cells: U937, Cancer cells: Total cells, Cancer cells: TME cells, TME cells, haMSC: HUVECs, haMSC: U937, HUVEC: U937, haMSC + HUVEC, haMSC + U937, HUVEC + U937, Cancer cells + haMSC, Cancer cells + HUVECs, Cancer cells + U937, haMSC: Total cells, HUVEC: Total cells, U937: Total cells, Cancer cell type).

Compiled data was then grouped by drug treatment and saved in different files that were then read into RStudio v1.4.1093 with R version 4.1 for use in model generation. The median absorbance value for each drug treatment was calculated and used as a threshold to assign each replicate a "high" or "low" response label. After appending the response label to the dataset, it was converted into the "Factor" datatype for use as the prediction variable. The normalized absorbance values (and any other parameters that were not needed) were then trimmed from the dataset.

### Machine learning model generation

The trimmed dataset was then split into a training set (75% of the samples) and a test set (25% of the samples). At this point, the seed was set at "123" in order to facilitate repeatable runs of the model. First, the training set was used to optimize the number of trees for the random forest to generate and the number of parameters to consider at each node split. Those optimal values were then used as inputs in the "**randomForest()**" function with the training set as the dataset to build the model and the test set in the test set slot. After running the model, the variable importance (quantified as mean decrease in Gini impurity) was saved, receiver operating characteristic (ROC) curves were generated, and AUC values were calculated to quantify model performance on the training and test sets for each drug. The ROC plots the true positive rate against the false positive rate at every possible threshold value. The AUC represents the probability of the model making a correct prediction. An AUC of 1.0 indicates the model is correct every time; an AUC of 0.5 indicates the model has the same performance as a random predictor.

## Data availability

Data generated during the current study are available from the corresponding author on reasonable request.

## Code availability

No codes have been generated in this work.

Received: 26 September 2024; Accepted: 25 June 2025;
Published online: 19 August 2025

## References

1. Matsuo, K. et al. Uptake and outcomes of neoadjuvant chemotherapy among US patients with less common epithelial ovarian carcinomas. *JAMA Netw. Open* **6**, e2318602 (2023).
2. Matulonis, U. A. et al. Ovarian cancer. *Nat. Rev. Dis. Prim.* **2**, 16061 (2016).
3. Millstein, J. et al. Prognostic gene expression signature for high-grade serous ovarian cancer. *Ann. Oncol.* **31**, 1240–1250 (2020).
4. Burdett, N. L. et al. Multiomic analysis of homologous recombination-deficient end-stage high-grade serous ovarian cancer. *Nat. Genet.* **55**, 437–450 (2023).
5. Lisio, M. A., Fu, L., Goyeneche, A., Gao, Z. H. & Telleria, C. High-grade serous ovarian cancer: basic sciences, clinical and therapeutic standpoints. *Int. J. Mol. Sci.* **20**, https://doi.org/10.3390/ijms20040952 (2019).
6. Chen, G. M. et al. Consensus on molecular subtypes of high-grade serous ovarian carcinoma. *Clin. Cancer Res.* **24**, 5037–5047 (2018).
7. Davidson, N. R. et al. Molecular subtypes of high-grade serous ovarian cancer across racial groups and gene expression platforms. *Cancer Epidemiol. Biomark. Prev.* **33**, 1114–1125 (2024).
8. Konecny, G. E. et al. Prognostic and therapeutic relevance of molecular subtypes in high-grade serous ovarian cancer. *J. Natl. Cancer Inst.* **106**, https://doi.org/10.1093/jnci/dju249 (2014).
9. Talhouk, A. et al. Development and validation of the gene expression predictor of high-grade serous Ovarian carcinoma molecular subTYPE (PrOTYPE). *Clin. Cancer Res.* **26**, 5411–5423 (2020).
10. Tothill, R. W. et al. Novel molecular subtypes of serous and endometrioid ovarian cancer linked to clinical outcome. *Clin. Cancer Res.* **14**, 5198–5208 (2008).
11. Way, G. P. et al. Comprehensive cross-population analysis of high-grade serous ovarian cancer supports no more than three subtypes. *G3* **6**, 4097–4103 (2016).
12. Palmirotta, R., Silvestris, E., D'Oronzo, S., Cardascia, A. & Silvestris, F. Ovarian cancer: novel molecular aspects for clinical assessment. *Crit. Rev. Oncol. Hematol.* **117**, 12–29 (2017).
13. Hornburg, M. et al. Single-cell dissection of cellular components and interactions shaping the tumor immune phenotypes in ovarian cancer. *Cancer Cell* **39**, 928–944.e926 (2021).
14. Izar, B. et al. A single-cell landscape of high-grade serous ovarian cancer. *Nat. Med.* **26**, 1271–1279 (2020).

15. Olalekan, S., Xie, B., Back, R., Eckart, H. & Basu, A. Characterizing the tumor microenvironment of metastatic ovarian cancer by single-cell transcriptomics. *Cell Rep.* **35**, 109165 (2021).
16. Kommoss, S. et al. Bevacizumab may differentially improve ovarian cancer outcome in patients with proliferative and mesenchymal molecular subtypes. *Clin. Cancer Res.* **23**, 3794–3801 (2017).
17. Cascio, S. et al. Cancer-associated MSC drive tumor immune exclusion and resistance to immunotherapy, which can be overcome by Hedgehog inhibition. *Sci. Adv.* **7**, eabi5790 (2021).
18. Coffman, L. G. et al. Human carcinoma-associated mesenchymal stem cells promote ovarian cancer chemotherapy resistance via a BMP4/HH signaling loop. *Oncotarget* **7**, 6916–6932 (2016).
19. Raghavan, S. et al. Carcinoma-associated mesenchymal stem cells promote chemoresistance in ovarian cancer stem cells via PDGF signaling. *Cancers* **12**, https://doi.org/10.3390/cancers12082063 (2020).
20. Duluc, D. et al. Tumor-associated leukemia inhibitory factor and IL-6 skew monocyte differentiation into tumor-associated macrophage-like cells. *Blood* **110**, 4319–4330 (2007).
21. Hagemann, T. et al. Ovarian cancer cells polarize macrophages toward a tumor-associated phenotype. *J. Immunol.* **176**, 5023–5032 (2006).
22. Ning, Y. et al. Co-culture of ovarian cancer stem-like cells with macrophages induced SKOV3 cells stemness via IL-8/STAT3 signaling. *Biomed. Pharmacother.* **103**, 262–271 (2018).
23. Raghavan, S., Mehta, P., Xie, Y., Lei, Y. L. & Mehta, G. Ovarian cancer stem cells and macrophages reciprocally interact through the WNT pathway to promote pro-tumoral and malignant phenotypes in 3D engineered microenvironments. *J. Immunother. Cancer* **7**, 190 (2019).
24. Steitz, A. M. et al. Tumor-associated macrophages promote ovarian cancer cell migration by secreting transforming growth factor beta induced (TGFBI) and tenascin C. *Cell Death Dis.* **11**, 249 (2020).
25. Zhu, X. et al. Macrophages derived exosomes deliver miR-223 to epithelial ovarian cancer cells to elicit a chemoresistant phenotype. *J. Exp. Clin. Cancer Res.* **38**, 81 (2019).
26. Cheng, H., Wang, Z., Fu, L. & Xu, T. Macrophage polarization in the development and progression of ovarian cancers: an overview. *Front. Oncol.* **9**, 421 (2019).
27. Fessler, E., Borovski, T. & Medema, J. P. Endothelial cells induce cancer stem cell features in differentiated glioblastoma cells via bFGF. *Mol. Cancer* **14**, 157 (2015).
28. Lu, J. et al. Endothelial cells promote the colorectal cancer stem cell phenotype through a soluble form of Jagged-1. *Cancer Cell* **23**, 171–185 (2013).
29. McCoy, M. G. et al. Endothelial cells promote 3D invasion of GBM by IL-8-dependent induction of cancer stem cell properties. *Sci. Rep.* **9**, 9069 (2019).
30. Kourou, K., Exarchos, T. P., Exarchos, K. P., Karamouzis, M. V. & Fotiadis, D. I. Machine learning applications in cancer prognosis and prediction. *Comput Struct. Biotechnol. J.* **13**, 8–17 (2015).
31. Huang, S. et al. Applications of support vector machine (SVM) learning in cancer genomics. *Cancer Genom. Proteom.* **15**, 41–51 (2018).
32. Adam, G. et al. Machine learning approaches to drug response prediction: challenges and recent progress. *npj Precis. Oncol.* **4**, 19 (2020).
33. Yu, K. H. et al. Predicting ovarian cancer patients' clinical response to platinum-based chemotherapy by their tumor proteomic signatures. *J. Proteome Res.* **15**, 2455–2465 (2016).
34. Yuan, B. et al. CellBox: interpretable machine learning for perturbation biology with application to the design of cancer combination therapy. *Cell Syst.* **12**, 128–140.e124 (2021).
35. Yu, K. H. et al. Deciphering serous ovarian carcinoma histopathology and platinum response by convolutional neural networks. *BMC Med.* **18**, 236 (2020).
36. Zhan, F. et al. A multimodal radiomic machine learning approach to predict the LCK expression and clinical prognosis in high-grade serous ovarian cancer. *Sci. Rep.* **13**, 16397 (2023).
37. Hamada, K. et al. A deep learning-based assessment pipeline for intraepithelial and stromal tumor-infiltrating lymphocytes in high-grade serous ovarian carcinoma. *Am. J. Pathol.* **194**, 1272–1284 (2024).
38. Kawakami, E. et al. Application of artificial intelligence for preoperative diagnostic and prognostic prediction in epithelial ovarian cancer based on blood biomarkers. *Clin. Cancer Res.* **25**, 3006–3015 (2019).
39. Khatun, M. S., Hasan, M. M. & Kurata, H. PreAIP: computational prediction of anti-inflammatory peptides by integrating multiple complementary features. *Front. Genet.* **10**, https://doi.org/10.3389/fgene.2019.00129 (2019).
40. Ahn, B. et al. Histopathologic image-based deep learning classifier for predicting platinum-based treatment responses in high-grade serous ovarian cancer. *Nat. Commun.* **15**, 4253 (2024).
41. Jayatilake, S. M. D. A. C. & Ganegoda, G. U. Involvement of machine learning tools in healthcare decision making. *J. Healthc. Eng.* **2021**, https://doi.org/10.1155/2021/6679512 (2021).
42. Desbois, M. et al. Integrated digital pathology and transcriptome analysis identifies molecular mediators of T-cell exclusion in ovarian cancer. *Nat. Commun.* **11**, https://doi.org/10.1038/s41467-020-19408-2 (2020).
43. Huang, C. et al. Machine learning predicts individual cancer patient responses to therapeutic drugs with high accuracy. *Sci. Rep.* **8**, 16444 (2018).
44. Hasan, M. K., Alam, M. A., Das, D., Hossain, E. & Hasan, M. Diabetes prediction using ensembling of different machine learning classifiers. *IEEE Access* **8**, 76516–76531 (2020).
45. Qi, Y. in *Ensemble Machine Learning: Methods and Applications* (eds Zhang, C. & Ma, Y.) 307–323 (Springer, 2012).
46. Olbrecht, S. et al. High-grade serous tubo-ovarian cancer refined with single-cell RNA sequencing: specific cell subtypes influence survival and determine molecular subtype classification. *Genome Med.* **13**, https://doi.org/10.1186/s13073-021-00922-x (2021).
47. Qian, J. et al. A pan-cancer blueprint of the heterogeneous tumor microenvironment revealed by single-cell profiling. *Cell Res.* **30**, 745–762 (2020).
48. Xu, J. et al. Single-cell RNA sequencing reveals the tissue architecture in human high-grade serous ovarian cancer. *Clin. Cancer Res.* **28**, 3590–3602 (2022).
49. Xu, S. et al. Discovery of an orally active small-molecule irreversible inhibitor of protein disulfide isomerase for ovarian cancer treatment. *Proc. Natl. Acad. Sci. USA* **109**, 16348–16353 (2012).
50. Grande, F., Aiello, F., Garofalo, A. & Neamati, N. Identification and preclinical evaluation of SC144, a Novel pyrroloquinoxaline derivative with broad-spectrum anticancer activity. *Mini Rev. Med. Chem.* **16**, 644–650 (2016).
51. McLean, K. et al. Leukemia inhibitory factor functions in parallel with interleukin-6 to promote ovarian cancer growth. *Oncogene* **38**, 1576–1584 (2019).
52. Lee, M. X. & Tan, D. S. Weekly versus 3-weekly paclitaxel in combination with carboplatin in advanced ovarian cancer: Which is the optimal adjuvant chemotherapy regimen?. *J. Gynecol. Oncol.* **29**, e96 (2018).
53. Raghavan, S. et al. Personalized medicine-based approach to model patterns of chemoresistance and tumor recurrence using ovarian cancer stem cell spheroids. *Clin. Cancer Res.* **23**, 6934–6945 (2017).
54. Silva, I. A. et al. Aldehyde dehydrogenase in combination with CD133 defines angiogenic ovarian cancer stem cells that portend poor patient survival. *Cancer Res.* **71**, 3991–4001 (2011).
55. Nowak, M. & Klink, M. The role of tumor-associated macrophages in the progression and chemoresistance of ovarian cancer. *Cells* **9**, https://doi.org/10.3390/cells9051299 (2020).

56. Yang, J. et al. Adipocytes promote ovarian cancer chemoresistance. *Sci. Rep.* **9**, 13316 (2019).
57. Le Naour, A. et al. Tumor cells educate mesenchymal stromal cells to release chemoprotective and immunomodulatory factors. *J. Mol. Cell Biol.* **12**, 202–215 (2020).
58. Zamora, A. et al. Paclitaxel induces lymphatic endothelial cells autophagy to promote metastasis. *Cell Death Dis.* **10**, 956 (2019).
59. Bocci, G., Di Paolo, A. & Danesi, R. The pharmacological bases of the antiangiogenic activity of paclitaxel. *Angiogenesis* **16**, 481–492 (2013).
60. Michailidou, M. et al. Microvascular endothelial cell responses in vitro and in vivo: modulation by zoledronic acid and paclitaxel?. *J. Vasc. Res.* **47**, 481–493 (2010).
61. Winkler, J., Abisoye-Ogunniyan, A., Metcalf, K. J. & Werb, Z. Concepts of extracellular matrix remodelling in tumour progression and metastasis. *Nat. Commun.* **11**, 5120 (2020).
62. Xu, S., Grande, F., Garofalo, A. & Neamati, N. Discovery of a novel orally active small-molecule gp130 inhibitor for the treatment of ovarian cancer. *Mol. Cancer Ther.* **12**, 937–949 (2013).
63. Liang, R. et al. STAT3 signaling in ovarian cancer: a potential therapeutic target. *J. Cancer* **11**, 837–848 (2020).
64. Sakellaropoulos, T. et al. A Deep learning framework for predicting response to therapy in cancer. *Cell Rep.* **29**, 3367–3373.e3364 (2019).
65. Lin, L. et al. STAT3 is necessary for proliferation and survival in colon cancer-initiating cells. *Cancer Res.* **71**, 7226–7237 (2011).
66. Cheng, C. C. et al. STAT3 exacerbates survival of cancer stem-like tumorspheres in EGFR-positive colorectal cancers: RNAseq analysis and therapeutic screening. *J. Biomed. Sci.* **25**, 60 (2018).
67. Chung, S. S. & Vadgama, J. V. Curcumin and epigallocatechin gallate inhibit the cancer stem cell phenotype via down-regulation of STAT3-NFκB signaling. *Anticancer Res.* **35**, 39–46 (2015).
68. Schwede, M. et al. The impact of stroma admixture on molecular subtypes and prognostic gene signatures in serous ovarian cancer. *Cancer Epidemiol. Biomark. Prev.* **29**, 509–519 (2020).
69. Lo Gullo, R., Eskreis-Winkler, S., Morris, E. A. & Pinker, K. Machine learning with multiparametric magnetic resonance imaging of the breast for early prediction of response to neoadjuvant chemotherapy. *Breast* **49**, 115–122 (2020).
70. Yin, J. Y. et al. Prediction models for platinum-based chemotherapy response and toxicity in advanced NSCLC patients. *Cancer Lett.* **377**, 65–73 (2016).
71. Pan, X. & Ma, X. A novel six-gene signature for prognosis prediction in ovarian cancer. *Front. Genet.* **11**, 1006 (2020).
72. Yuzhalin, A. E., Urbonas, T., Silva, M. A., Muschel, R. J. & Gordon-Weeks, A. N. A core matrisome gene signature predicts cancer outcome. *Br. J. Cancer* **118**, 435–440 (2018).
73. Krishnamurthy, S. et al. Endothelial cell-initiated signaling promotes the survival and self-renewal of cancer stem cells. *Cancer Res.* **70**, 9969–9978 (2010).
74. Le Naour, A. et al. Tumor cells educate mesenchymal stromal cells to release chemoprotective and immunomodulatory factors. *J. Mol. Cell Biol.* **12**, 202–215 (2020).
75. Wen, Y., Guo, Y., Huang, Z., Cai, J. & Wang, Z. Adipose-derived mesenchymal stem cells attenuate cisplatin-induced apoptosis in epithelial ovarian cancer cells. *Mol. Med. Rep.* **16**, 9587–9592 (2017).
76. Raghavan, S. et al. Personalized medicine based approach to model patterns of chemoresistance and tumor recurrence using ovarian cancer stem cell spheroids. *Clin. Cancer Res.* https://doi.org/10.1158/1078-0432.CCR-17-0133 (2017).
77. Bregenzer, M. et al. The role of the tumor microenvironment in CSC enrichment and chemoresistance: 3D co-culture methods. *Methods Mol. Biol.* **2424**, 217–245 (2022).
78. Burkhard, K. M. & Mehta, G. Multicellular tumoroids for investigating cancer stem-like cells in the heterogeneous tumor microenvironment. *Methods Mol. Biol.* **2777**, 99–122 (2024).


## Acknowledgements

We gratefully acknowledge the contributions of ovarian cancer patients and advocates in donating tissues, raising awareness, and lobbying for ovarian cancer research. We are grateful to the departments of Materials Science and Biomedical Engineering at the University of Michigan for fostering an inclusive environment for current and future scientists and researchers of all educational levels.

## Author contributions

All authors edited and approved the final version of the manuscript. The author contributions following CREDIT guidelines are as follows: conceptualization, Michael E. Bregenzer, Pooja Mehta, Geeta Mehta; data curation, Michael E. Bregenzer, Pooja Mehta, Kathleen Burkhard; formal analysis, Michael E. Bregenzer, Pooja Mehta, Kathleen Burkhard, Geeta Mehta; funding acquisition, Geeta Mehta; investigation, Michael E. Bregenzer, Pooja Mehta, Kathleen Burkhard; methodology, Michael E. Bregenzer, Pooja Mehta, Kathleen Burkhard, Geeta Mehta; project administration, Geeta Mehta; resources, Geeta Mehta; supervision, Geeta Mehta; validation, Michael E. Bregenzer, Pooja Mehta, Kathleen Burkhard; writing—original draft, Michael E. Bregenzer, Pooja Mehta, Kathleen Burkhard, Geeta Mehta; writing—review and editing, Kathleen Burkhard, Geeta Mehta.

## Competing interests

The authors declare no competing interests.

## Additional information

**Supplementary information** The online version contains supplementary material available at https://doi.org/10.1038/s44385-025-00032-y.

**Correspondence** and requests for materials should be addressed to Geeta Mehta.